JOURNAL OF SOLID STATE CHEMISTRY 108, 211–218 (1994)

New Data on Chemical Delithiation of $Li_xNi_{2-x}O_2$ ($0.6 < x < 1$)

R. Stoyanova and E. Zhecheva

Institute of General and Inorganic Chemistry, Bulgarian Academy of Sciences, 1113 Sofia, Bulgaria

Received January 6, 1993; in revised form April 30, 1993; accepted May 7, 1993

New data on acid delithiation of lithium–nickel oxides, $Li_xNi_{2-x}O_2$ ($0.6 < x < 1$), are obtained using EPR of low-spin Ni^{3+} ions, magnetic susceptibility measurements, and thermal analysis. It is shown that short-range and long-range cation order in the solid solutions $Li_xNi_{2-x}O_2$ specify their behavior toward acids. For $Li_xNi_{2-x}O_2$ oxides ($0.6 < x < 0.9$), where partial cation order occurs, acids remove lithium and impurity nickel ions from the LiO_2-layers, but do not attack Ni^{2+} and Ni^{3+} ions, which are segregated in the neighboring (111) cubic planes. For $Li_xNi_{2-x}O_2$ oxides ($x > 0.9$), where long-range cation order is developed, the extraction of lithium and impurity nickel ions proceeds concomitantly with partial exchange between lithium from the LiO_2-layers and protons from the acid solution. The different chemical compositions of acid-treated oxides $Li_xNi_{2-x}O_2$ ($0.6 < x < 0.9$) and $Li_xNi_{2-x}O_2$ ($0.9 < x < 1$) are manifested by their thermochemical properties up to 200°C: for the partially ordered oxides ($0.6 < x < 0.9$), reduction of highly oxidized nickel ions and cation redistribution occur within the initial structural framework, whereas for the layered oxides ($x > 0.9$), dehydration processes also take place.

1. INTRODUCTION

Stoichiometric $LiNiO_2$ and $LiCoO_2$ are isostructural and possess a hexagonal α-$NaFeO_2$-type structure built up from LiO_2-and MO_2-layers, in which the lithium and nickel (or cobalt) ions are located in trigonally deformed octahedral sites (1). Using X-ray diffraction and Rietveld profile refinement, Dahn and co-workers (2) have shown that, in contrast to $LiCoO_2$, some cation disorder exists in $LiNiO_2$, i.e., "nonperfect" LiO_2- and NiO_2-layers are formed. As is well known, the lithium–nickel oxides are usually prepared as nonstoichiometric $Li_xNi_{2-x}O_2$ ($0.6 < x < 1$), owing to the difficult oxidation of Ni^{2+} to Ni^{3+} (3–6). The Ni^{2+} ions frustrate the layered crystal structure and, in the limiting case, when $x_c = 0.62$ (2), short-range cation order only is preserved within the framework of the cubic structure. According to EPR studies of low-spin N^{3+} ions (7, 8), we have shown recently that in the oxides with critical lithium amount ($x \approx 0.6$) part of the Li^+, Ni^{3+}, and Ni^{2+} ions segregate in appropriate neighboring (111) planes of the cubic structure (7). This ion segregation (designed as "sandwich" type clusters) disappears at $x \geq 0.96$, where the hexagonal structure is achieved and the Ni^{2+} ions are statistically distributed in the LiO_2- and NiO_2-layers (8).

Lithium–nickel and lithium–cobalt oxides are among the promising candidates for electrode materials in secondary lithium batteries (9–11) because lithium is easy to remove electrochemically from the layered crystal structure. The perturbation of the LiO_2-layers by impurity nickel ions in $Li_xNi_{2-x}O_2$ hinders the ionic transport, which results in bad performance of the electrochemical cells (11). Using Rietveld analysis of XRD data, Tirado and co-workers (12) have established that acids act as delithizing agents towards $Li_xNi_{2-x}O_2$, i.e., in a similar way as electrochemical deintercalation (9) does. We have shown that acid digestion of layered $LiCoO_2$ yields metastable layered $Li_{1-x-y}H_yCoO_2$ ($x < 0.55$, $x + y < 1$) phases (13).

In the present paper we report new data on chemical delithiation of $Li_xNi_{2-x}O_2$ ($0.6 < x < 1$) obtained by EPR of low-spin Ni^{3+}, magnetic susceptibility measurements, and thermal analysis. For the sake of comparison, the acid delithiation of a cobalt-substituted lithium–nickel oxide having a layered structure has also been studied.

2. EXPERIMENTAL

Four kinds of samples were investigated: three $Li_xNi_{2-x}O_2$ samples with $0.6 < x < 1$ and $Li_x(Ni_{0.8}Co_{0.2})_{2-x}O_2$ with $x = 0.9$.

Solid Li_2CO_3 was added with intensive stirring to a 75% solution of $Ni(NO_3)_2$ (and $Co(NO_3)_2$, $Ni/(Ni + Co) = 0.8$), taken in an atomic ratio of $Li/Ni\ (+Co) = 1.05/1$. The water from this mixture was then evaporated at 100°C until a dry residue consisting of $LiNO_3$ and nickel (and cobalt) hydroxide nitrate were obtained. This dry residue was heated at 220°C until the complete evolution of the nitrogen oxides, then ground and heated at 500°C for 6 h, ground again, pelleted, and heated at 850°C for 30 h. Samples with the compositions $Li_{0.64}Li_{1.36}O_2$ and $Li_{0.92}(Ni_{0.8}Co_{0.2})_{1.08}O_2$ were obtained.

Lithium–nickel oxides with a higher lithium content

0022-4596/94 $6.00

were synthesized by a solid state reaction between NiO and LiOH. Nickel oxide prepared from nickel hydroxide carbonate at 350°C was impregnated with a saturated LiOH solution. The mixture was dried and heated to the melting point of LiOH (400°C) for 6 h, then heated at 650°C for 18 h under oxygen or in air. The samples obtained had the compositions $Li_{0.92}Ni_{1.08}O_2$ (under oxygen) and $Li_{0.83}Ni_{1.17}O_2$ (in air). For the sake of convenience, the four samples are denoted LNO-D, LNO-PO, LNO-O, and LMO-O, which correspond to $Li_{0.64}Ni_{1.36}O_2$, $Li_{0.83}Ni_{1.17}O_2$, $Li_{0.92}Ni_{1.08}O_2$, and $Li_{0.92}(Ni_{0.8}Co_{0.2})_{1.08}O_2$, respectively. The symbols D, PO, and O are chosen for a disordered, a partially ordered, and an ordered solid solution, respectively.

The acid delithiation of the oxides studied was achieved by treating 2 g of each sample at room temperature with 100 ml of 0.1, 1, and 8 *N* HCl for 24, 2, and 0.5 h, respectively. The duration of treatment was experimentally determined with a view to attaining at least 50–60% dissolution of the sample. The solid residues were then dried at room temperature. The acid-treated samples are denoted by LNO-*x*/A, where *x* represents D, PO and O.

The lithium content was determined by atomic absorption analysis, the total nickel and cobalt content was established by complexometric titration, and the mean oxidation state of Ni and Co ions was found by iodometric titration.

The phase composition of the samples was controlled by powder X-ray analysis with a Philips spectrometer using Cu K_α radiation. The unit cell parameters were determined by least squares fits to all Bragg's peaks positions. The specific surface area of the samples was determined by the BET method.

The DTA and TG measurements were performed with a Stanton Redcroft apparatus (England) in platinum crucibles with a diameter of 5 mm at 20–500°C and a heating rate of 10°C/min.

The EPR spectra of the samples were recorded with an ERS-300 (Bruker) spectrometer between 4.2 and 300 K.

The magnetic susceptibility was measured by the Faraday method at 100–600 K.

3. RESULTS AND DISCUSSION

The X-ray patterns of the initial oxides are indexed to the trigonal space group $R\bar{3}m$ (Figs. 1a and 1b). According to refs. (2, 5, 12), the variation in the relative intensities of the (003) and (101) diffraction lines reveals the different cation distributions in the initial solid solutions. For LNO-D with a lower lithium content (Fig. 1a), the weak (003) peak indicates only a short-range cation order; for LNO-PO (Fig. 1a), the increase in the (003) and (101) intensities shows a long-range cation correlation instead of a short-range order; and, for LNO-O (Fig. 1b), the structure is close to the hexagonal layered α-$NaFeO_2$ (ordered cubic structure). The X-ray patterns of the acid treated oxides are similar (in terms of line positions) to those of the initial oxides, indicating preservation of the structural framework during acid treatment.

The acid treatment of the oxides affects the chemical composition (Fig. 2a, Table 1) and the unit cell dimensions (Fig. 2b, Table 1). For the sake of comparison, the data of Tirado and co-workers (12) concerning acid treatment of lithium–nickel oxides ($Li_{0.92}Ni_{1.08}O_2$-A and $Li_{0.68}Ni_{1.32}O_2$-B) are also given in Fig. 2. After the acid treatment, the lithium amount decreases and the mean oxidation degree of the metal ions increases as acid concentration increases (Fig. 2a and Table 1). It must be emphasized that strong acids (above 1 *N*) only extract lithium from the oxide with a short-range ordered structure (LNO-D), but on the other hand, strong acids dissolve the oxide with a long-range ordered structure (LNO-O). The decrease in the *a*-parameter with the increase of the oxidation state of Ni (and Co) (Fig. 2b) reflects the appearance of Ni^{4+} and/or Co^{4+} with smaller ionic radii in the MO_2-layers (NiO_2- and $Ni_{0.8}Co_{0.2}O_2$-layers). The expansion of the unit cell along the *c*-axis (Fig. 2c, Table 1) reflects the decrease in the electrostatic binding energy in the lithium-depleted layers.

The acid treatment of the oxides also leads to a broadening of the XRD lines and to an increase of the specific surface area (Figs. 3a and 3b, Table 1). Hence, the line broadening can be attributed to a reduction of cristallinity during the acid treatment. Only for layered LNO-O, the strong broadening of the XRD lines with the increase of the scattering angle (Fig. 3a) indicates that, in addition to particle size effects, strains (resulting from stacking disorder, cation clustering, composition inhomogeneity, etc.) also contribute to the XRD linewidths. It should be mentioned that the same result has been observed during the acid treatment of $LiCoO_2$ (13), when the acid removal of lithium is accompanied by proton insertion. Furthermore, the increase in I_{003}/I_{104} and decrease in $I_{10\bar{2}.006}/I_{101}$ (Figs. 3c and 3d, Table 1) for the acid-treated samples suggests that, within the initial structural framework, the cation distribution is modified. Tirado and co-workers (12) have explained the change in I_{003}/I_{104} by a preferred extraction of lithium ions (and nickel ions) from the LiO_2-slabs. From these results it appears that the acid treatment of LNO-D, LNO-PO, and LMO-O proceeds differently in comparison to that of LNO-O: acids remove mainly lithium and some nickel ions from $Li_xNi_{2-x}O_2$ (Figs. 3c and 3d); but for layered LNO-O, lithium delithiation causes considerable strains (Fig. 3a), as is the case of layered $LiCoO_2$ (13).

EPR studies are fulfilled in order to elucidate the behavior of the NiO_2-layers during the acid treatment of $Li_xNi_{2-x}O_2$. Recently, we have revealed the relationship be-

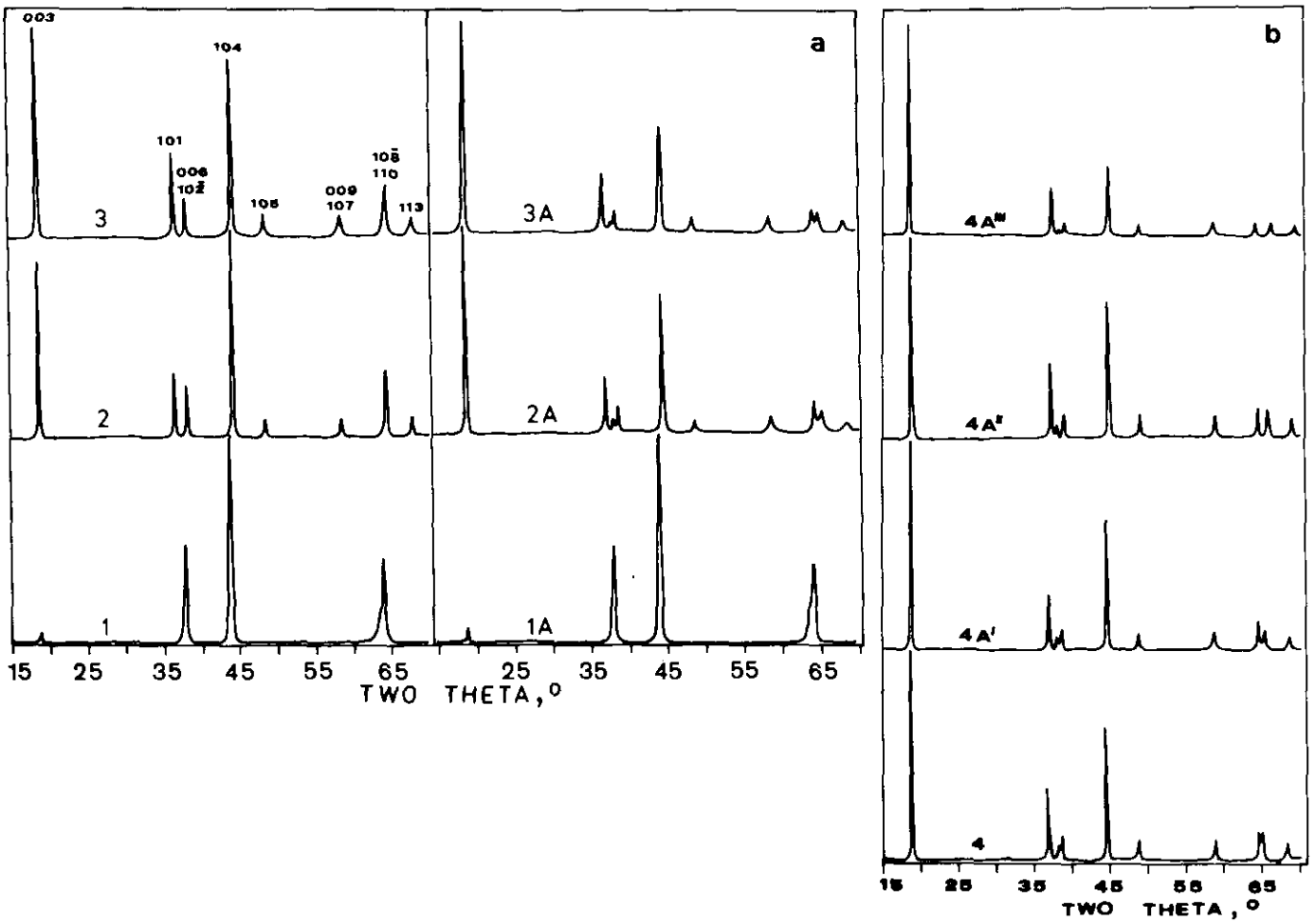

FIG. 1. (a) X-ray patterns of initial and acid-treated $Li_xNi_{2-x}O_2$: LNO-D (1, 1A), LNO-PO (2, 2A), and LNO-O (3, 3A). The Miller indices of the Bragg peaks are given near each line. Acid concentration: 8 *N* HCl for LNO-D and LNO-PO, 1 *N* HCL for LNO-O. (b) X-ray patterns of initial LMO-O (4) and LMO-O treated with 0.1, 1, and 8 *N* HCl (4A′, 4A″, and 4A‴ resp).

tween the cation distribution in $Li_xNi_{2-x}O_2$ ($0.6 \leq x < 1$) and the parameters of low-spin Ni^{3+} ions (7, 8). For $Li_xNi_{2-x}O_2$ with $x \approx 0.6$, where short-range cation order only exists, the antiferromagnetic interactions between the segregated Ni^{2+} and Ni^{3+} ions determine a ferrimagnetic transition at 210 K, which is reflected in the critical narrowing of the Lorentzian EPR line in the vicinity of the transition temperature, as well as in the splitting of this signal below 210 K (7). For nearly stoichiometric $Li_xNi_{2-x}O_2$ ($x = 0.96$), where long-range cation order exists, the interlayer ferromagnetic Ni^{3+}–Ni^{3+} interactions and the Jahn–Teller effect of low-spin Ni^{3+} (d^7) give rise to a complex temperature dependence of the EPR linewidth between 9 and 400 K: narrowing up to 100 K; broadening up to 35 K; and narrowing up to 9 K (8). Figure 4 presents the temperature behavior of the EPR linewidth of the isotropic signal ($g = 2.137$) of low-spin Ni^{3+} ions in the initial and acid-treated oxides. Along with X-ray data, EPR data support the evidence for different cation distributions in the initial oxides. For LNO-D, LNO-PO, and LMO-O, and Ni^{2+} and Ni^{3+} ions segregate into neighboring (111) crystal planes as evidenced by the critical narrowing of the EPR linewidth in the vicinity of the ferrimagnetic transition temperature (210, 160, and 35 K, respectively). The decrease of the ferrimagnetic transition temperature, as the lithium content increases, reflects the competition between the long-range Li^+–Ni^{3+} order and Ni^{2+}–Ni^{3+} segregation. Further details on short-range cation order in $Li_xNi_{2-x}O_2$ revealed by EPR are in progress (15). When Ni^{2+} ions are statistically distributed in the LiO_2- and NiO_2-layers, the temperature dependence of the EPR linewidth is drastically changed, as one can see for layered LNO-O (Fig. 4).

After the acid-treatment, the EPR spectra show sharply outlined magnetic transitions (Fig. 4), this suggesting a composition homogeneity. The acid treatment of the LNO-D, LNO-PO, and LMO-O oxides does not change their ferrimagnetic transition temperatures (Fig. 4), which

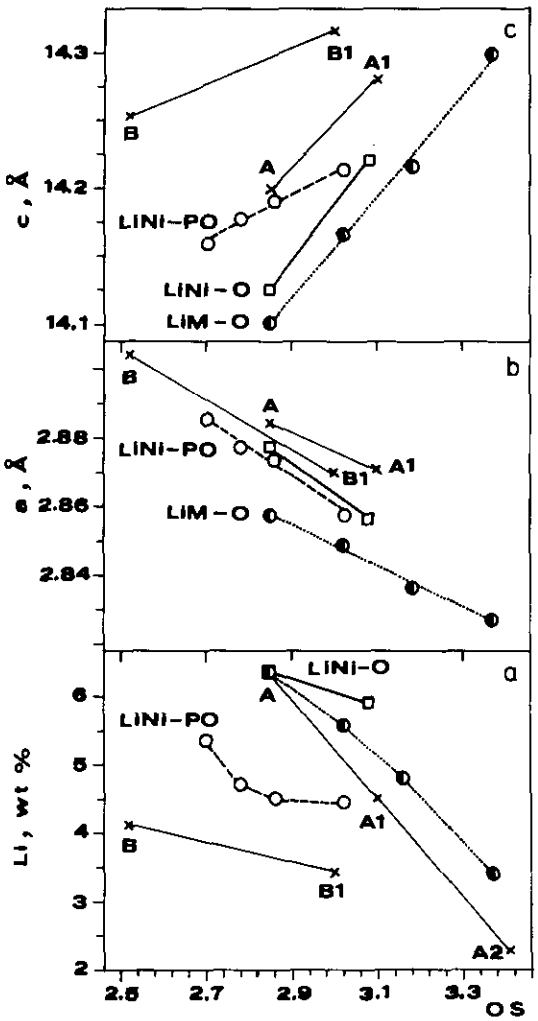

FIG. 2. (a) Lithium amount (wt%) versus the mean oxidation state of metal ions (Ni + Co) after acid treatment of LNO-PO (dashed line), LNO-O (full line), and LMO-O (dotted line). (b) Unit cell parameter a (Å) versus the mean oxidation state after acid treatment of LNO-PO (dashed line), LNO-O (full line), and LMO-O (dotted line). (c) Unit cell parameter c (Å) versus the mean oxidation state during acid treatment of LNO-PO (dashed line), LNO-O (full line), and LMO-O (dotted line). The data of Tirado and co-workers (12) concerning acid treatment of $Li_{0.92}Ni_{1.08}O_2$ (A) and $Li_{0.68}Ni_{1.32}O_2$ (B) are also given.

explicitly shows that the Ni^{2+}–Ni^{3+} clusters are not attacked by the acid. The slight broadening of the EPR signal of acid-treated LNO-D, LNO-PO and LMO-O (Fig. 4) most probably reflects lattice strains induced by lithium extraction. In contrast to the above samples, acid delithiation of layered LNO-O causes a significant broadening of the EPR signal of the Ni^{3+} ions in the NiO_2-layers, but the temperature dependence of the EPR line width remains the same. These results can be interpreted by stabilization of low-spin Ni^{4+} in the NiO_2-layers: on the one hand, the diamagnetic Ni^{4+} ions ($S = 0$) dilute the magnetically concentrated NiO_2-layers, which results in broadening of the EPR signal of Ni^{3+}, and, on the other hand, the amount of Ni^{4+} must be sufficiently small to cause no change in the temperature dependence of the EPR linewidth. Thus, the NiO_2-layers are only slightly distorted during the acid delithiation. In this case, because of the two-dimensional crystal lattice, EPR data may complement X-ray results concerning strains induced by acid delithiation: it seems that the strains are mainly localized in the LiO_2-layers. As in the case of $LiCoO_2$ (13), one may suppose that proton insertion during acid delithiation would stress the depleted LiO_2-layers.

TABLE 1

Lithium Amount (wt%), Oxidation State of Nickel Ions (OS), Unit Cell Dimensions (a and c), Linewidth of the (003) and (104) Diffraction Lines ($\Delta 2\theta_{003}$ and $\Delta 2\theta_{104}$(°)), Specific Surface Area (S (m^2/g)), and I_{003}/I_{104} Intensity Ratio for the Initial and Acid-Treated $Li_{0.64}Ni_{1.36}O_2$ (LNO-D and LNO-D/A)

	LNO-D	LNO-D/A
Li (wt%)	3.70	3.63
OS	2.30	2.35
$a \pm 0.004$ (Å)	2.900	2.896
$c \pm 0.01$ (Å)	14.21	14.19
$\Delta 2\theta_{003}$ (°)	0.300	0.343
$\Delta 2\theta_{104}$ (°)	0.418	0.487
S (m^2/g)	1	10
I_{003}/I_{104}	0.17	0.22

To check the supposition about proton insertion during acid delithiation of LNO-O, Fig. 5 presents the DTA and TG curves of acid-treated oxides. All the samples studied decompose irreversibly between 150 and 500°C (Fig. 5). As one can see, the thermal behavior of layered LNO-O differs from that of LNO-PO and LMO-O. The thermal decomposition of LNO-O/A starts at the lowest temperature: there is an endothermic effect and the corresponding weight loss between 125 and 200°C, indicating the H_2O evolution, while the larger weight loss is observed between 200 and 400°C and the corresponding thermal effect is not well resolved. Thermal decomposition of LNO-PO/A and the cobalt-substituted LMO-O/A is accomplished in two steps: an exo effect and the corresponding weight loss are spread over a wide temperature range up to 300°C (50–250°C and 50–300°C for LNO-PO and LMO-O, respectively), while between 300 and 450°C, an endo effect and the main weight loss take place.

In attempt to elucidate the low-temperature effects (endothermic and exothermic effects at 180 and 200°C for LNO-O/A and LNO-PO/A, respectively), Figs. 6 and 7 show the X-ray diffraction patterns and the EPR spectra of acid-treated LNO-O/A and LNO-PO/A heated for 15 min at 180°C. The X-ray patterns of the heated samples

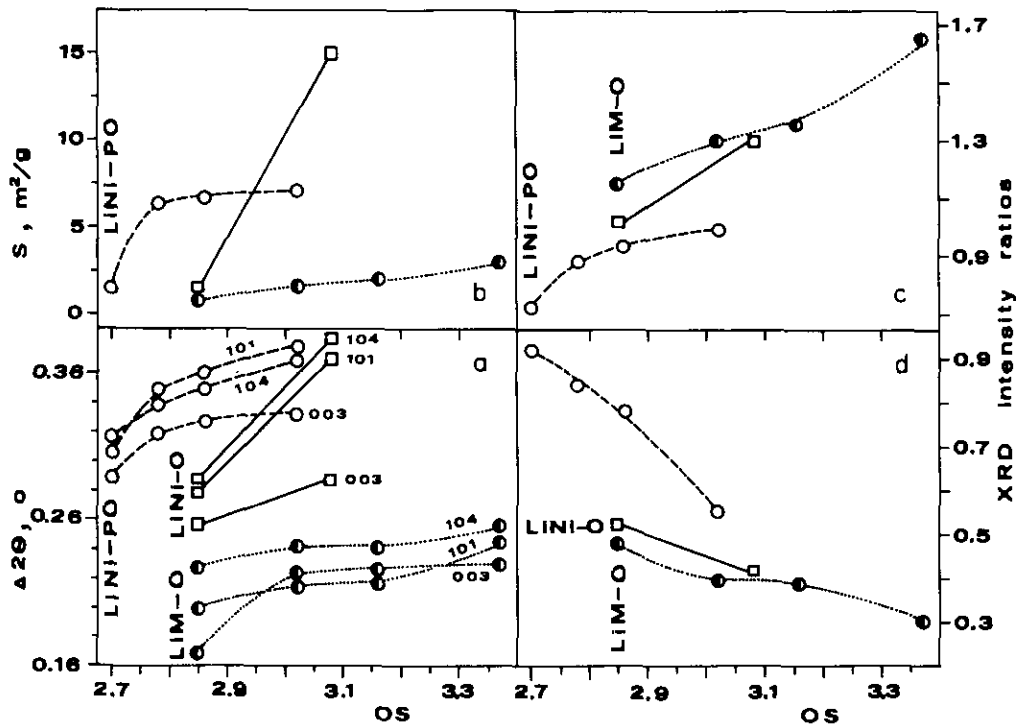

FIG. 3. (a) XRD linewidths ($\Delta 2\theta$) at half maximum intensity of (003), (101), and (104) peaks versus the mean oxidation state during acid treatment of LNO-PO, LNO-O, and LMO-O. (b) Specific surface area (S) of LNO-PO, LNO-O, and LMO-O versus the mean oxidation state of metal ions (Ni + Co). (c) XRD intensity ratio I_{003}/I_{104} versus the mean oxidation state after the acid treatment of LNO-PO, LNO-O, and LMO-O. (d) XRD intensity ratio I_{101}/I_{104} versus the mean oxidation state after acid treatment of LNO-PO, LNO-O, and LMO-O. Sample notation as in Fig. 2.

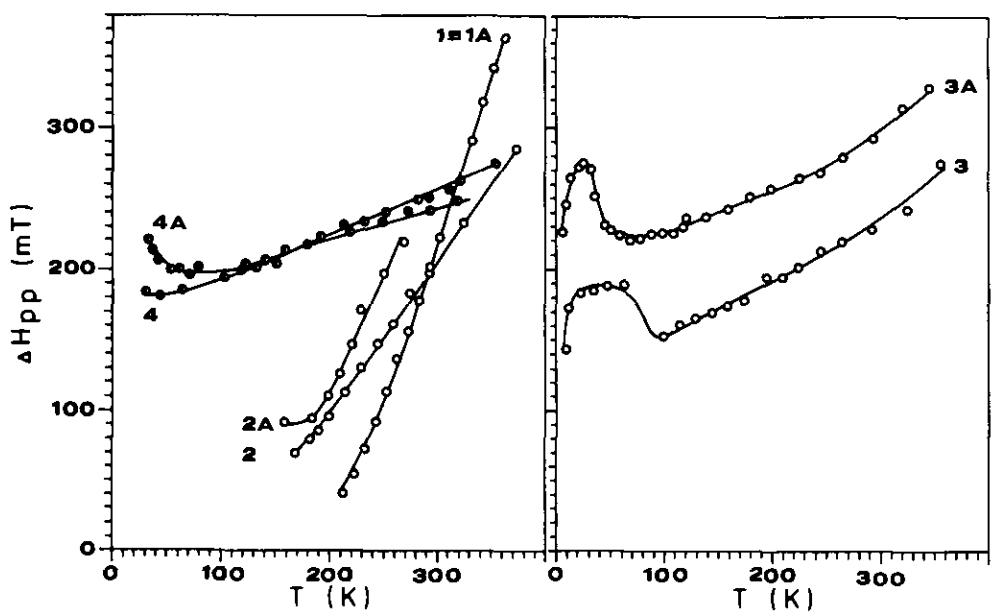

FIG. 4. Dependence of the EPR peak-to-peak linewidth (ΔH_{pp}) of low-spin Ni^{3+} on the registration temperature. Sample notation: (1) and (1A), LNO-D and LNO-D/A; (2) and (2A), LNO-PO and LNO-PO/A; (3) and (3A), LNO-O and LNO-O/A; (4) and (4A), LMO-O and LMO-O/A.

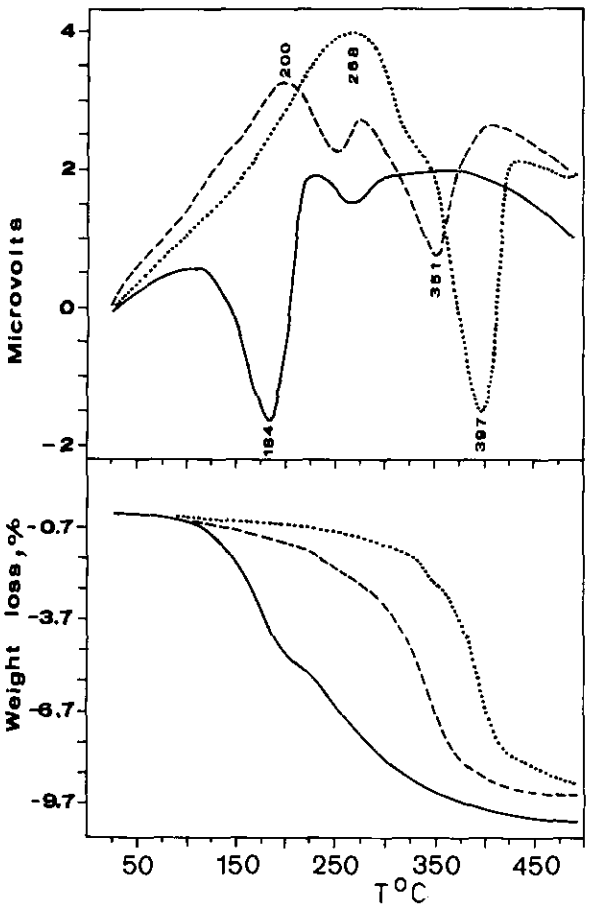

FIG. 5. DTA and TG profiles of acid-treated oxides: LNO-PO/A (dashed line), LNO-O/A (full line), and LMO-O (dotted line).

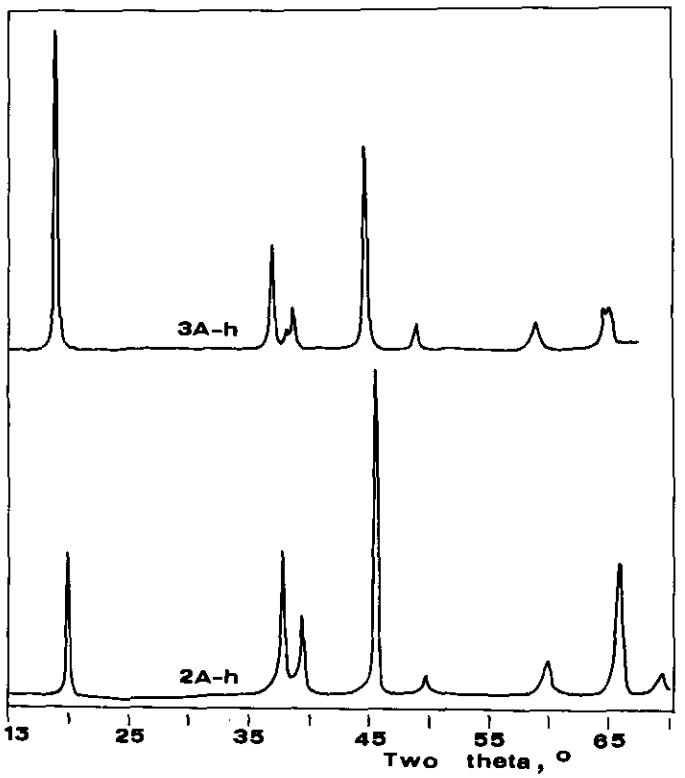

FIG. 6. X-ray patterns of LNO-PO/A (2A-h) and LNO-O/A (3A-h) heated at 180°C.

are similar to these of the initial samples (Fig. 6), i.e., the initial structure is preserved during heating up to 200°C. For both samples, the unit cell dimensions and the relative intensities of the XRD lines change (Table 2): a increases and c decreases, which indicates reduction of the highly oxidized ions, while the decrease in I_{003}/I_{104} reveals a cation redistribution within the same structural framework. In contrast to LNO-PO, during the endothermic decomposition of layered LNO-O/A, the XRD line widths decrease slightly, irrespective of the increase of the specific surface area (Table 2), which means that the strains, concentrated in the LiO_2-layers, are annihilated during the endothermic decomposition of LNO-O. This result supports the supposition that the low-temperature endothermic process for LNO-O is due to dehydration. Moreover, the XRD data are consistent with the EPR data (Fig. 7): the temperature behavior of the EPR line width of the heated samples is changed. For the LNO-O/A and LNO-PO/A, the EPR signal is narrowed at about 180 and 240 K, respectively, which demonstrates strong ferrimagnetic interactions, i.e., segregation of Ni^{2+} and Ni^{3+} ions in appropriate neighbouring layers. During the heating of LNO-PO/A up to 200°C, the redistribution of lithium and nickel ions leads to further segregation of Ni^{2+}–Ni^{3+} in neighbouring crystal planes, which is visualized by an increase in the critical temperature from 160 to 240 K

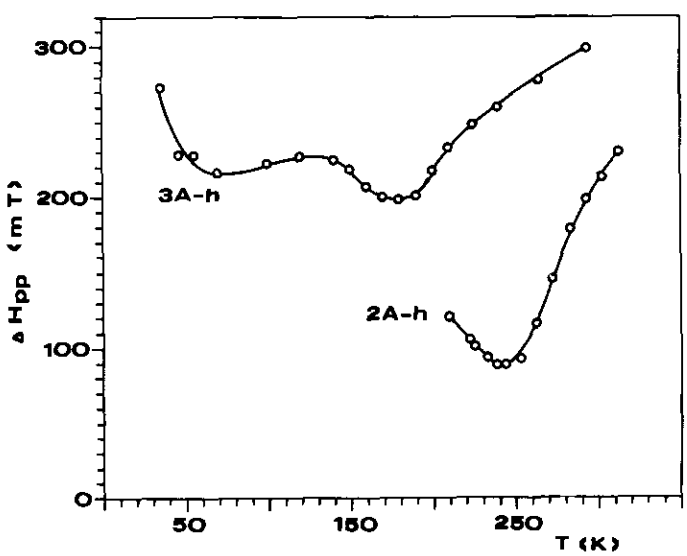

FIG. 7. Temperature dependence of EPR peak-to-peak linewidth for LNO-PO/A (2A-h) and LNO-O/A (3A-h) heated at 180°C.

TABLE 2

Unit Cell Dimensions (a and c), Linewidth of the (003), (104), and (101) Diffraction Lines ($\Delta 2\theta_{003}$, $\Delta 2\theta_{104}$, and $\Delta 2\theta_{101}$), Specific Surface Area (S), and I_{003}/I_{104} and $I_{10\bar{2},006}/I_{101}$ Intensity Ratios for the Acid-Treated $Li_{0.83}Ni_{1.17}O_2$ (LNO-PO/A) and $Li_{0.94}Ni_{1.06}O_2$ (LNO-O/A) as Well as LNO-PO/A and LNO-O/A Heated at 180°C for 15 min (LNO-PO/A-h and LNO-O/A-h)

	LNO-PO		LNO-O	
	LNO-PO/A	LNO-PO/A-h	LNO-O/A	LNO-O/A-h
$a \pm 0.0004$ (Å)	2.857	2.872	2.857	2.860
$c \pm 0.008$ (Å)	14.212	14.181	14.222	14.203
$\Delta 2\theta_{003}$ (°)	0.332	0.386	0.289	0.290
$\Delta 2\theta_{104}$ (°)	0.368	0.421	0.386	0.365
$\Delta 2\theta_{101}$ (°)	0.379	0.415	0.371	0.356
S (m^2/g)	7.0	7.3	15	20
I_{003}/I_{104}	0.96	0.35	1.34	1.21
$I_{10\bar{2},006}/I_{101}$	0.51	0.59	0.40	0.36

(Figs. 4 and 7). During the heating of LNO-O/A up to 200°C, dehydration and reduction processes initiate a Ni^{2+}–Ni^{3+} segregation within the layered structure (critical temperature 180 K, Fig. 7). The lack of a distant signal splitting below the critical temperatures for the two samples manifests some inhomogeneity in the chemical composition of the oxides heated up to 200°C.

The differences between the magnetic properties of stoichiometric $LiNiO_2$ (3, 4, 8, 14) and non-stoichiometric $Li_xNi_{2-x}O_2$ (3, 4, 7) permit clarifying the thermochemical behavior of acid delithiated oxides above 200°C. The temperature dependence of the magnetic susceptibility (χ) for initial LNO-O (Fig. 8) is described between 150 and 600 K by the Curie–Weiss law with a Curie constant $C = 0.45$ and a Weiss constant $\theta = 80$ K, as is described in Refs. (8, 14), while for LNO-PO, the Curie–Weiss law is not obeyed due to the relatively high temperature of ferrimagnetic transition ($T_C = 160$ K). For the acid-treated oxides, the magnetic susceptibility changes reversibly between 150 and 300 K, but the Curie–Weiss law is not obeyed. The decrease in χ for the acid-treated oxides as compared with χ for the initial oxides between 150 and 300 K (Fig. 8) refects both disappearance of Ni^{2+} and generation of diamagnetic Ni^{4+} during the acid delithiation. A peculiarity of the thermal behaviour of the delithiated oxides is the irreversible change of the magnetic susceptibility above 50°C due to thermal decomposition of the samples. First, the increase of χ above 130 and 160°C for LNO-O/A and LNO-PO/A, respectively, clarifies the reduction of Ni^{4+} and the redistribution of paramagnetic ions such as Ni^{2+} and Ni^{3+}. In addition, the different shapes of the heating curves of LNO-O/A and LNO-PO/A demonstrate different thermochemical properties due to exchange of lithium with protons in the case of LNO-O. The cooling curves for both samples have the same shape and are not

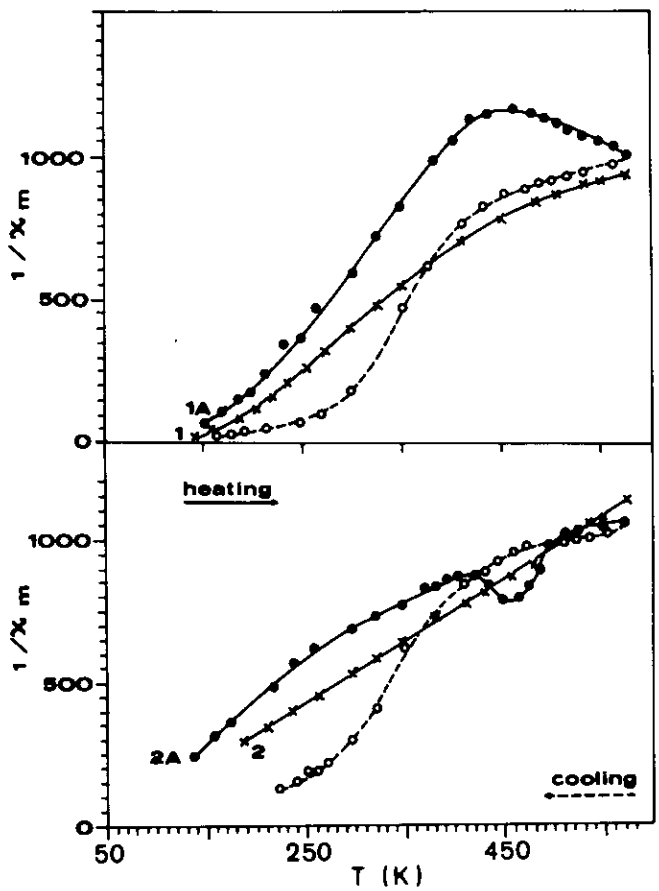

FIG. 8. Temperature changes of the magnetic susceptibilities of LNO-PO (1), LNO-PO treated with 8 N HCl (1A), LNO-O (2), and LNO-O treated with 1 N HCl (2A).

TABLE 3
The Final Chemical Composition of the Acid-Treated Oxides as Calculated from the Chemical Analysis and the Weight Loss Analysis: $Li_xNi_{2-x}O_2 \rightarrow Li_{x-z-y}H_yNi_{2-x_a}O_2$

	LNO-PO			LMO-O			LNO-O		
HCl (N)	z	y	$2\text{-}x_a$	z	y	$2\text{-}x_a$	z	y	$2\text{-}x_a$
Fresh	0	0	1.18	0	0	1.08	0	0	1.08
0.01	0.10	0	1.18	0.12	0	1.06			
1.0	0.14	0	1.16	0.24	0	1.05	0.10	0.10	1.0
8.0	0.17	0	1.11	0.42	0	1.04			

described by the Curie-Weiss law: the sharp increase of χ below 295 K reveals strong exchange interactions between Ni^{2+} and Ni^{3+}. The similarity in the cooling curves of the two samples indicates that the products of thermal decomposition of acid-treated LNO-O/A and LNO-PO/A above 200°C are similar. The X-ray patterns and EPR spectra of LNO-PO/A and LNO-O/A, heated up to 450°C, show several lithium–nickel oxide phases with ordered ($x \geq 0.6$) structures. Summarizing the data from XRD-analysis, EPR, and magnetic susceptibility measurements, it can be concluded that the broad exothermic effect observed during heating of LNO-PO/A up to 200°C manifests both reduction of highly oxidized nickel ions (Ni^{4+}) and redistribution of lithium and nickel within the initial structure, while the endothermic effect observed during heating of LNO-O/A up to 200°C manifests the dehydration process. Hence, from chemical analysis and weight loss curves we are able to calculate the chemical compositions of the acid-treated oxides, which are shown in Table 3.

4. CONCLUSIONS

Two effects can be deduced when lithium-transition metal oxides are treated with acids: lithium deintercalation and exchange of lithium with protons from the acid solution. For example, the acid acts toward $LiMn_2O_4$ as a delithizing agent (16, 17) and towards $LiCoO_2$ as a delithizing and a hydrolyzing agent simultaneously (13). During acid treatment of $Li_xNi_{2-x}O_2$ ($0.6 < x < 1$), where transition from a short-range order to a long-range order is realized, new phenomena are established: delithiation of $Li_xNi_{2-x}O_2$ proceeds only in the LiO_2-layers and is accompanied by removal of the statistically distributed impurity nickel ions from the same layers. The segregated Ni^{2+}–Ni^{3+} ions remain as a stable configuration towards the acid action. In addition, the acid delithiation of $Li_xNi_{2-x}O_2$ ($x > 0.9$) with a long-range cation ordered structure proceeds by partial exchange between the lithium ions from the depleted LiO_2-layers and the proton from the acid solution. It is worth noting that with the cobalt-substituted lithium–nickel oxide, when Ni^{2+} and Ni^{3+} tend to segregate, no insertion of protons from the acid solution is observed in spite of the "X-ray" long-range cation order.

ACKNOWLEDGMENTS

The authors express their gratitude to Professor D. Reinen and Professor C. Friebel for helpful discussions and comments. Financial support from the National Research Foundation of Bulgaria (Contract CH 83/1991) is gratefully acknowledged.

REFERENCES

1. T. A. Hewston and B. L. Chamberland, *J. Phys. Chem. Solids* **48,** 97 (1987).
2. W. Li, J. N. Reimers, and J. R. Dahn, *Phys. Rev. B* **46,** 3236 (1992).
3. J. B. Goodenough, D. G. Wickman, and W. J. Croft, *J. Phys. Chem. Solids* **5,** 107 (1958).
4. V. W. Bonger, H. Bade, and W. Klemm, *Z. Anorg. Allg. Chem.* **333,** 188 (1964).
5. J. R. Dahn, U. von Sacken, and C. A. Michael, *Solid State Ionics* **44,** 87 (1990).
6. V. Berbenni, V. Massarotti, D. Capsoni, R. Riccardi, A. Marini, and A. Antolini, *Solid State Ionics* **48,** 101 (1991).
7. R. Stoyanova, E. Zhecheva, and S. Angelov, *Solid State Ionics* **59,** 17 (1993).
8. R. Stoyanova, E. Zheheva, and C. Friebel, *J. Phys. Chem. Solids* **54,** 9 (1993).
9. M. G. S. R. Thomas, W. I. F. David, J. B. Goodenough, and P. Groves, *Mater. Res. Bull.* **20,** 1137 (1985).
10. A. LeCerf, M. Broussely, and J. P. Gabano, *Eur. Patent Appl.* EP345707 (1989).
11. J. R. Dahn, U. von Sacken, M. W. Juskow, and H. Al-Janaby, *J. Electrochem. Soc.* **138,** 2207 (1991).
12. J. Morales, C. Peres-Vicente, and J. L. Tirado, *Mater. Res. Bull.* **25,** 623 (1990).
13. E. Zhecheva and R. Stoyanova, submitted for publication.
14. J. P. Kemp, P. A. Cox, and J. W. Hodby, *J. Phys.: Condensed Matter* **2,** 6699 (1990).
15. E. Zhecheva, R. Stoyanova, and C. Friebel, submitted for publication.
16. J. C. Hunter, *J. Solid State Chem.* **39,** 142 (1981).
17. J. B. Goodenough, M. M. Thackeray, W. I. F. David, and P. G. Bruce, *Rev. Chim. Miner.* **21,** 435 (1984).